Mode of opening of an oceanic pull-apart: The 20°N Basin along the Owen Fracture Zone (NW Indian Ocean)

Mathieu Rodriguez,[1,2,3] Nicolas Chamot-Rooke,[1] Marc Fournier,[2,3] Philippe Huchon,[2,3] and Matthias Delescluse[1]

[1]   Pull-apart basins are common features observed at releasing bends along major strike-slip faults. The formation and structural evolution of such basins have mostly been investigated in the continental domain and by sandbox laboratory experiments or numerical models. Here we present recently acquired multibeam bathymetry, 3.5 kHz echo sounder, and seismic profiles across the 20°N pull-apart Basin along the India-Arabia transform boundary, known as the Owen Fracture Zone (OFZ). Using nearby oceanic drilling (Deep Sea Drilling Project 222), we constrain the structural evolution of the basin since opening some 3 Myr ago. The 20°N Basin is large (90 km long and 35 km wide) despite limited transcurrent motion (~10 km). The first stage involved the formation of a step over along the OFZ and the subsequent isolation of a subsiding half graben. Extension and subsidence were further partitioned over three distinct subbasins separated by complex sets of transverse faults. The size of the basin was enhanced by gravity-driven collapse. The 20°N Basin has been a catchment for Indus turbidites since its opening, which provide a good record of syn-sedimentary deformation. The deformation related to the subsidence of the half graben mimics rollover structures commonly encountered in salt tectonics, suggesting that subsidence was accommodated by one or several décollement layers at depth. Despite a different rheological context, the subsurface structure of the nascent oceanic 20°N Basin is very similar to the more mature continental Dead Sea Basin along the Levant Fault, which also displays subbasins separated by transverse faults.

Citation: Rodriguez, M., N. Chamot-Rooke, M. Fournier, P. Huchon, and M. Delescluse (2013), Mode of opening of an oceanic pull-apart: The 20˚N Basin along the Owen Fracture Zone (NW Indian Ocean), *Tectonics*, *32*, doi:10.1002/tect.20083.

1.   Introduction

[2]   Pull-apart basins are topographic depressions commonly observed along strike-slip faults (see *Cunningham and Mann* [2007] for a synthesis). They occur in step over-releasing bend areas, either in transtensional or in pure strike-slip contexts [*Wu et al.*, 2010]. Pull-apart basins accommodate the transfer of slip between adjacent fault segments on both sides of the step over region, generating higher subsidence rates with respect to other types of basin [*Christie-Blick and Biddle*, 1985]. First studies on the Dead Sea Basin proposed a progressive size increase of the basin with increasing finite strike slip [*Aydin and Nur*, 1982; *Mann et al.*, 1983]. Subsequent works showed that the growth of the basin is accommodated by the coalescence of distinct subbasins driven by a gravity process together with subsidence localization through times

[*Ten Brink and Ben-Avraham*, 1989; *Ten Brink et al.*, 1993]. More recent studies of the San Andreas Fault System show that step over regions migrate along the main strike-slip fault [*Wakabayashi et al.*, 2004; *Wakabayashi*, 2007]. Either subsidence relocalization or migrating step overs involve the formation of transverse faults orthogonal or oblique to the main strike-slip direction. Although progressive structure development within pull-apart basins has been the focus of many analog modeling works [*Rahe et al.*, 1998; *Basile and Brun*, 1999; *Smit et al.*, 2008a, 2008b; *Wu et al.*, 2010], few field examples constrain the precise age or the relative chronology of such structure emplacement [*Ten Brink and Ben-Avraham*, 1989; *Carton et al.*, 2007; *Brothers et al.*, 2009].

[3]   The 20°N pull-apart Basin, named after its latitude, is situated in the Arabian Sea along the Owen Fracture Zone (hereafter OFZ), which is the currently active, pure strike-slip India-Arabia plate boundary (Figure 1) [*Fournier et al.*, 2011]. The 800 km long dextral strike-slip system connects the Makran subduction zone to the north to the Aden-Owen-Carlsberg triple junction to the south (Figure 1) [*Fournier et al.*, 2008a; *Fournier et al.*, 2010]. The OFZ closely follows a small circle about the Arabia-India rotation pole determined with GPS and seismicity data, which predicts pure strike-slip motion along the entire fracture zone [*Fournier et al.*, 2011], in contrast with the increasing transtension north of 18°N predicted by the MORVEL (Mid Ocean Ridge VELocity model) closure-enforced pole [*DeMets et al.*, 2010]. As indicated by

---

[1]Laboratoire de Géologie de l'Ecole normale supérieure, CNRS UMR 8538, Paris, France.
[2]Institut des Sciences de la Terre de Paris, CNRS UMR 7193, Université Pierre et Marie Curie, Paris, France.
[3]iSTeP, UMR 7193, CNRS, F-75005, Paris, France.

Corresponding author: M. Rodriguez, Laboratoire de Géologie de l'Ecole normale supérieure, CNRS UMR 8538, 24 rue Lhomond, 75005 Paris CEDEX, France. (rodriguez@geologie.ens.fr)
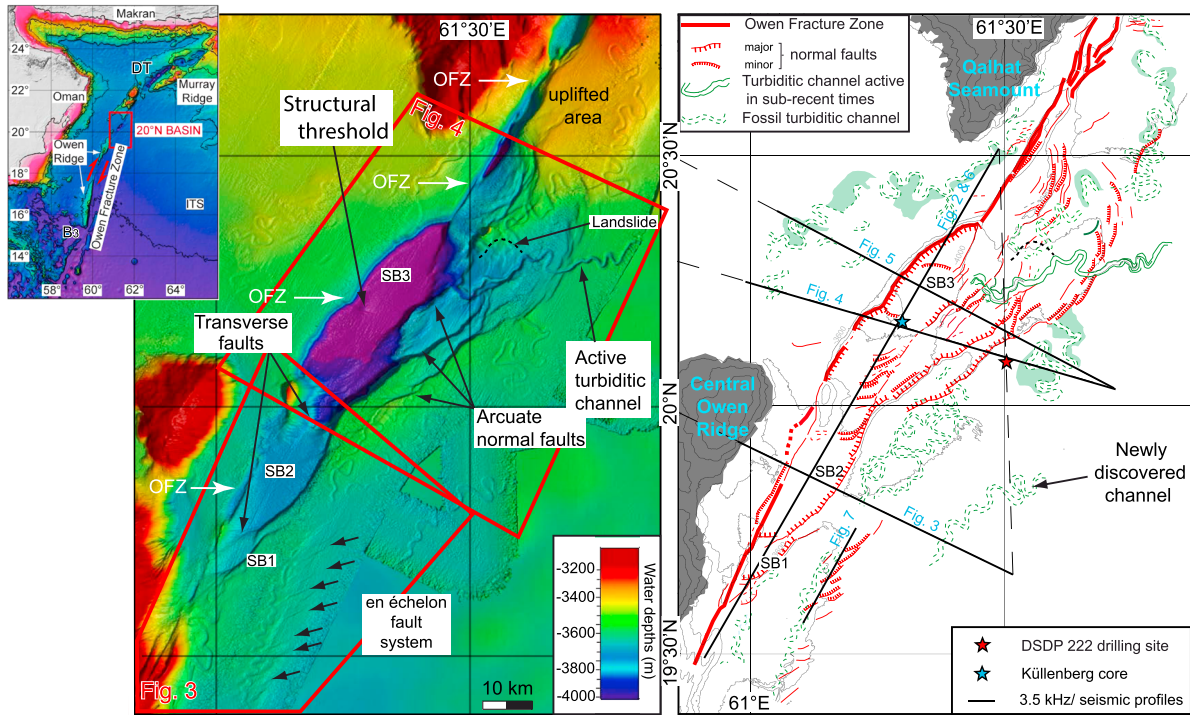
Figure 1. Multibeam map of the 20°N pull-apart basin and interpretative structural scheme, together with the location of seismic profiles, cores, and drilling available in the study area. Inset on the left-hand corner shows the regional framework of the 20°N Basin. B3: Beautemps-Beaupré Basin, DT: Dalrymple Trough, ITS: Indus Turbiditic System, OFZ: Owen Fracture Zone, SB: subbasin.

dextral strike-slip focal mechanisms of earthquakes, the Arabian plate moves northward slightly faster than the Indian plate with a relative motion of 3 ± 1 mm yr^{-1}, estimated independently from geodetic [*Reilinger et al.*, 2006; *Fournier et al.*, 2008b] and geological data [*DeMets et al.*, 1990, 1994, 2010]. The OFZ cuts through the Owen Ridge, a prominent relief affected by numerous submarine landslides [*Rodriguez et al.*, 2012, 2013]. Offsets of the Owen Ridge observed on the seafloor imply a finite dextral displacement of 10–12 km along the OFZ [*Fournier et al.*, 2008b, 2011]. Considering a steady motion of 3 ± 1 mm yr^{-1}, this indicates that the present-day trace of the OFZ has been active since at least 3–6 Ma.

[4] The mean depth of the surrounding seafloor indicates that the 20°N Basin cuts into thin crust, either oceanic or highly stretched continental. West, the substratum of the Owen Basin is a 6 km thick oceanic crust [*Barton et al.*, 1990] of Paleocene age according to deep-sea drillings [*Shipboard Scientific Party*, 1974, 1989]. East, magnetic anomaly A28 (63 Ma), formed at the onset of seafloor spreading at the Carlsberg Ridge, is identified up to 19°N [*Dyment*, 1998; *Royer et al.*, 2002; *Chaubey et al.*, 2002]. North of anomaly A28, magnetic anomalies have been tentatively identified as the oceanic lineations of the Gop Basin (A31 or A29 to A25, 69/64 to 56 Ma) [*Malod et al.*, 1997; *Collier et al.*, 2008; *Yatheesh et al.*, 2009]. The nature of the crust between the Arabian oceanic lithosphere and the Gop oceanic basin remains uncertain [*Calvès et al.*, 2011; *Armitage et al.*, 2011]. It may correspond to the Laxmi-Palatina Ridge, which is interpreted as a continental remnant separated from the Seychelles Bank during its breakup from India ~65 Ma ago [*Minshull et al.*, 2008; *Yatheesh et al.*, 2009;

Calvès et al., 2011]. The connection between these elements and the OFZ remains unstudied.

[5] *Fournier et al.* [2011] and *Rodriguez et al.* [2011] used multibeam bathymetry and 3.5 kHz echo sounder profiles to map the subsurface structure of the 20°N Basin. The 20°N Basin is a 90 km long and up to 35 km wide pull-apart basin, which developed in a 12 km wide step over between two major segments of the OFZ (Figure 1). The overall structure of the basin is asymmetric, with the OFZ as a steep master fault on the western side and a complex system of arcuate normal faults on the eastern sidewall. The 20°N Basin is divided in three distinct subbasins (labeled SB1, SB2, and SB3 in Figure 1) limited by transverse faults. Subbasins 1, 2, and 3 extend over 70, 340, and 590 km^2, respectively. The 20°N Basin deepens abruptly northward, as subbasins 1, 2, and 3 form relatively flat areas, respectively, 60, 100, and 360 m deep with respect to the nondepressed surrounding seafloor. A system of en echelon faults is observed on its southeastern side. An active turbiditic channel cuts through the arcuate fault system and feeds SB3, which has recorded the Indus deep-sea fan activity since the opening of the basin [*Rodriguez et al.*, 2011].

[6] The structural characteristics of the 20°N Basin raises several questions about the mode of pull-apart basin opening in an oceanic setting. First, the dimension of the 20°N Basin is much larger than the relative motion accommodated by the OFZ since its inception by almost 1 order of magnitude, thus invalidating some models [*Aydin and Nur*, 1982; *Petrunin and Sobolev*, 2006]. This raises the questions of how extensional deformation is distributed in a step over basin and what mechanism is responsible for the high amount of subsidence.
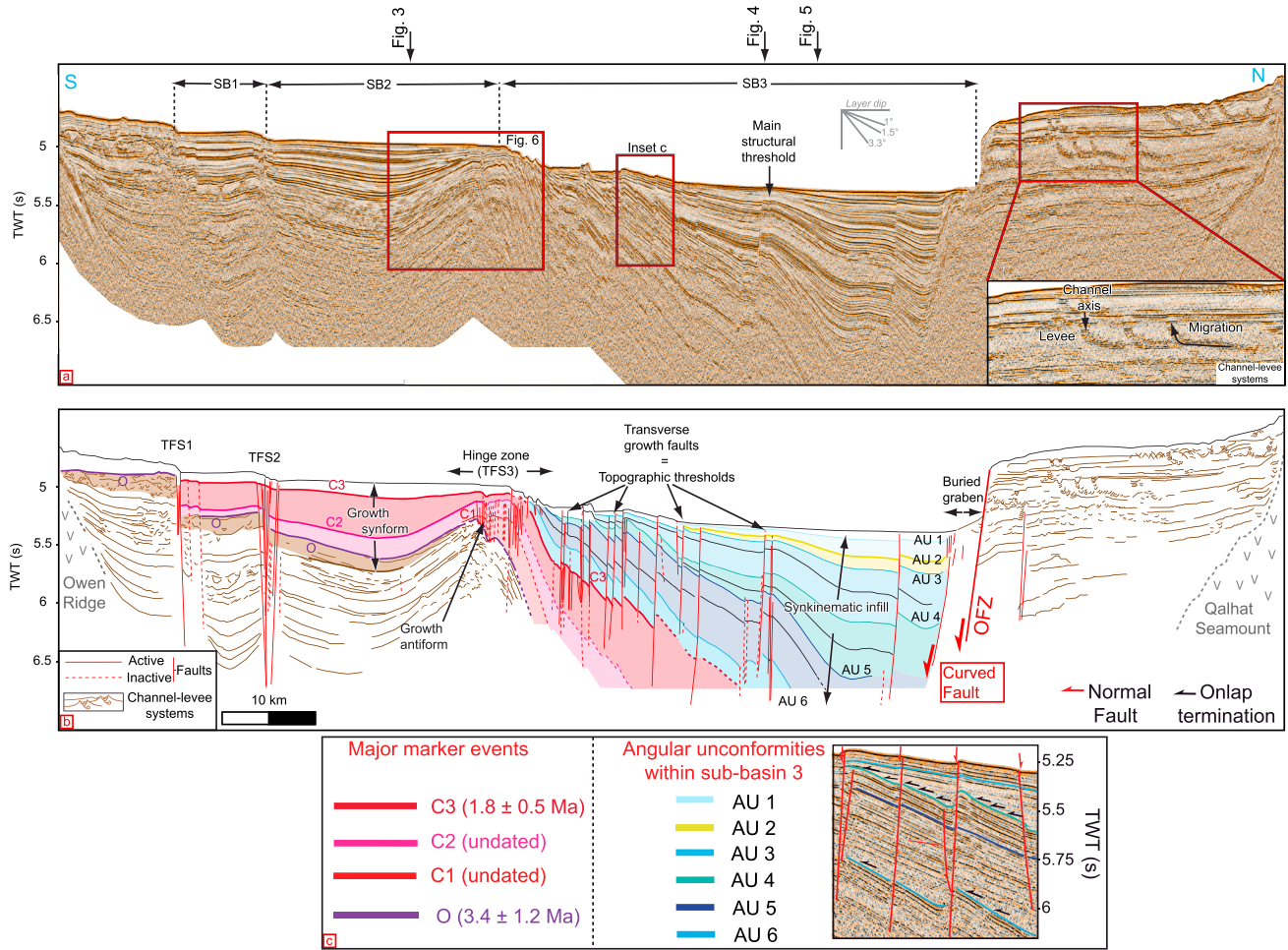
Figure 2. Longitudinal seismic line crossing the 20°N Basin (see Figure 1 for location). Inset shows a close view of migrating turbiditic channels. Inset c presents the horizons mapped in seismic section across the 20°N Basin and their stratigraphic significance. The 20°N Basin is composed of three subbasins labeled SB1, SB2, and SB3 from south to north. The subbasins are separated by Transverse Fault Systems (TFS).

Second, it remains unclear whether subbasins are still all active or not [*Rodriguez et al.*, 2011]. The origin of transverse faults within pull-apart basins, together with subsidence localization processes through times, are key processes in the structural evolution of pull-apart basins [*Ten Brink and Ben Avraham*, 1989; *Ben Avraham and Ten Brink*, 1989; *Smit et al.*, 2008a, 2008b].

[7] The aim of this study is to constrain the structural evolution of the 20°N Basin since its inception, through the analysis of newly acquired seismic lines. The close location of Deep Sea Drilling Project (DSDP) site 222, together with Küllenberg cores from *Bourget et al.* [2013], provide a good stratigraphic control on seismic lines (Figure 1). Seismic profiles document the nature of sedimentary deposits (in particular, pelagites versus turbidites), which are essential to the understanding of the active deformation in marine environments [e.g., *Barnes and Pondard*, 2010; *Pondard and Barnes*, 2010]. The tectonic activity and related topographic changes strongly influenced the course of distal Indus turbiditic channels as well as the emplacement of bottom current. Turbiditic and contouritic deposits provide good dated landmarks of the opening of the 20°N Basin. The structure of the 20°N Basin is compared with other pull-apart basins (with a particular emphasis over the Dead Sea Basin) and analog modeling studies [*Smit et al.*, 2008a, 2008b; *Brun and Mauduit*, 2008; *Dooley and Schreurs*, 2012].

2. Structure of the 20°N Pull-Apart Basin

2.1. Seismic Data Set

[8] Here we present a data set composed of four seismic lines (located on Figure 1), complementary documented by 3.5 kHz profiles collected during the OWEN (2009) and OWEN-2 (2012) cruises on board the R/V *Beautemps-Beaupré*. Seismic reflection profiles were shot using two GI air guns and a short 600 m long streamer allowing high-speed acquisition (10 knots) and a penetration of the order of ~2 s two-way travel time (TWT). The processing consisted in geometry setting, water-velocity normal moveout, stacking, water-velocity F-K domain post stack time migration, bandpass filtering (8–80 Hz), and automatic gain control. All profiles are displayed with a vertical exaggeration of 8 at the seafloor. Two-way travel times in the sediments were converted to depth using a lower 1530 and upper 1730 m s^{-1} bounds for the P wave velocity. This range of values covers safely the measurements performed in the same type
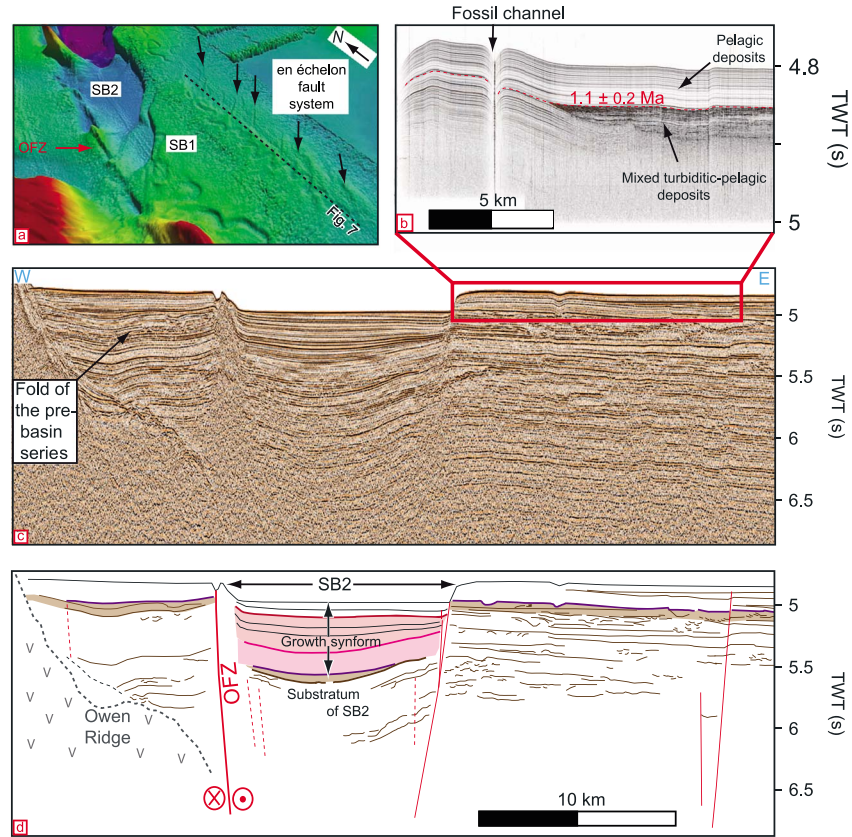
Figure 3. (a) A 3-D bathymetric view of the en echelon fault system near SB1 and SB2. (b) 3.5 kHz profiles crossing the channel dissected by 20° Basin faults. 1.1 ±0.2 Ma old turbiditic deposits overlying this channel come from an adjacent, unfaulted channel. (c) Seismic profile transverse to SB2 and (d) the related interpretation. See Figure 1 for location and Figure 2c for stratigraphic captions. OFZ: Owen Fracture Zone, SB: subbasin.

of pelagic sediments at other Ocean Drilling Program (ODP) and DSDP sites in the area [*Shipboard Scientific Party*, 1974, 1989]. Depth values are given with respect to the surrounding seafloor. In the following, sedimentary series before the opening of the 20°N Basin are referred to as the "substratum" of the 20°N Basin, which is employed in the sense of "prerift" series, in order to avoid the confusion with the oceanic basement of the Owen Ridge observed on several profiles. The reflectors picked on seismic profiles have been selected upon the base of seismic discontinuities that either reflect lithological changes, stratigraphic hiatuses, or tectonic deformation.

2.2. Architecture of the 20°N Basin

[9] A NNE-SSW-trending longitudinal profile crosses the three subbasins (SB1, SB2, and SB3) and provides a general picture of the 20°N Basin (Figure 2). The three subbasins are asymmetric and bounded by nonequidistant transverse faults systems (Figure 1). Three additional ESE-WNW seismic profiles (Figures 3–5) cut these transverse structures, allowing discussing their main structural characteristics and their relation with the eastern arcuate fault system. In the following, we describe the longitudinal structure of the 20°N Basin from south (SB1) to north (SB3), as well as the transverse structures of SB2 and SB3.

[10] The deep longitudinal structure of the 11 km long SB1 in Figure 2 shows reflectors tilted to the south below 5.3 s

(TWT), which contrasts with the flat reflectors above. At the seafloor, one single oblique normal fault bounds SB1 southward, but the longitudinal profile reveals additional normal growth faults buried below 5 s (TWT) (Figure 2).

[11] A set of transverse normal faults, clearly expressed at the seafloor, makes the junction with SB2. Although flat topped, SB2 displays a syncline structure at depth on both the longitudinal (Figure 2) and the transverse (Figure 3) profiles. The symmetry of SB2 indicates that west and east bounding faults accommodate nearly the same rate of subsidence (Figure 3). On the longitudinal profile, the tilt of the northern limb of SB2 is more pronounced than the southern limb, which is nearly flat (Figure 2). The increase of seismic horizons dip with depth on both transverse and longitudinal sections suggests that SB2 is a growth structure (i.e., the structure grows while simultaneously covered by sediments). Minor normal faulting is observed below 5.5 s (TWT) on the transverse profile (Figure 3). An anticline separates SB2 from SB3 (Figures 1 and 2), forming a hinge zone characterized by the progressive tilting of sedimentary layers on both of its limbs. Numerous nonequidistant transverse growth faults, characterized by the increase of their throw with depth, cut through the hinge zone. There, numerous faults observed at depth below 5.2 s (TWT) are not expressed at the seafloor (Figure 2), suggesting that they are inactive.
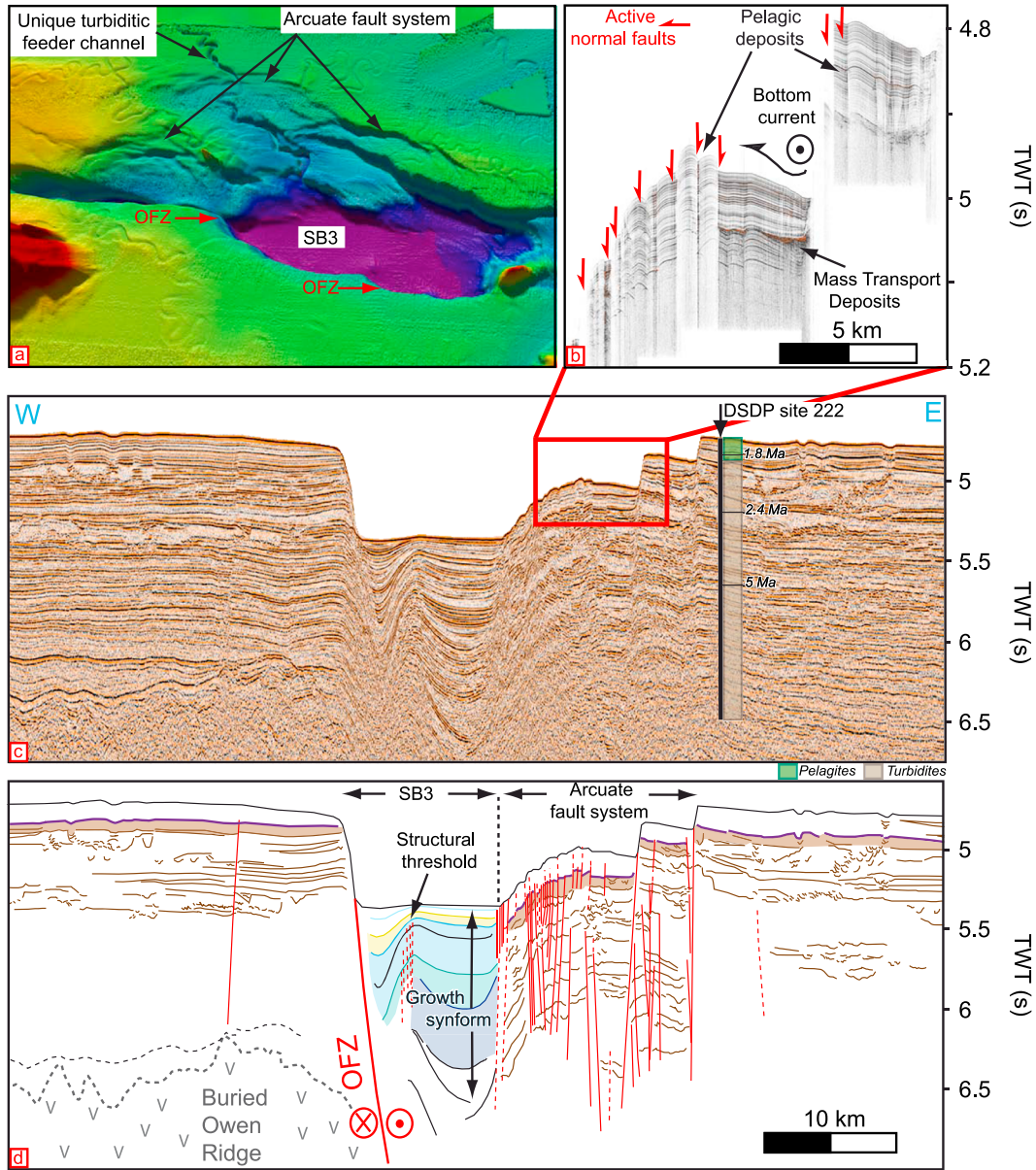
Figure 4. (a) A 3-D bathymetric view of SB3 and its arcuate normal fault system. (b) 3.5 kHz profile crossing the arcuate normal fault system. (c) Seismic line transverse to SB3 and (d) the related interpretation. DSDP site 222 documents a Pleistocene pelagic cover overlying Pliocene and Miocene turbidites from the Indus Fan [*Shipboard Scientific Party*, 1974]. See Figure 1 for location and Figure 2 for stratigraphic captions. OFZ: Owen Fracture Zone, SB: subbasin.

[12] SB3 is the largest of the three subbasins. It forms a half graben on the longitudinal section and a syncline on the transverse ones (Figures 4 and 5). This half graben is bounded to the north by the OFZ with a strong normal component there. The longitudinal fanning configuration of the turbiditic deposits in SB3 reflects its strong structural asymmetry, indicating that most of the subsidence is accommodated by the OFZ (Figure 2). The configuration of SB3 deposits is typical of a rollover anticline [*Cloos*, 1968; *Brun and Mauduit*, 2008]. At the hanging wall of the OFZ, 20°N Basin deposits have progressively buried a 4 km wide graben composed of Indus fan sediments, which is bounded by a transverse fault slightly expressed at the seafloor (Figures 1 and 2). Subsidence within SB3 is controlled by a set of numerous transverse growth faults that show a subtle expression at the seafloor (Figures 1 and 2). The growth fault activity is associated with the increasing tilt of the sedimentary layers. The rate of displacement of the transverse growth fault located at the latitude of 20°10′N is larger than the surrounding faults, which formed the main structural threshold within SB3 (Figure 2).

[13] The last main structural characteristic of SB3 is the dense network of arcuate faults on the eastern side of the basin (Figures 1, 4, and 5). The density of normal faults decreases toward the Indus plain. The offset of sedimentary layers cut by arcuate faults is roughly constant at depth. The entire arcuate normal fault system has accommodated over 500 m of distributed subsidence.
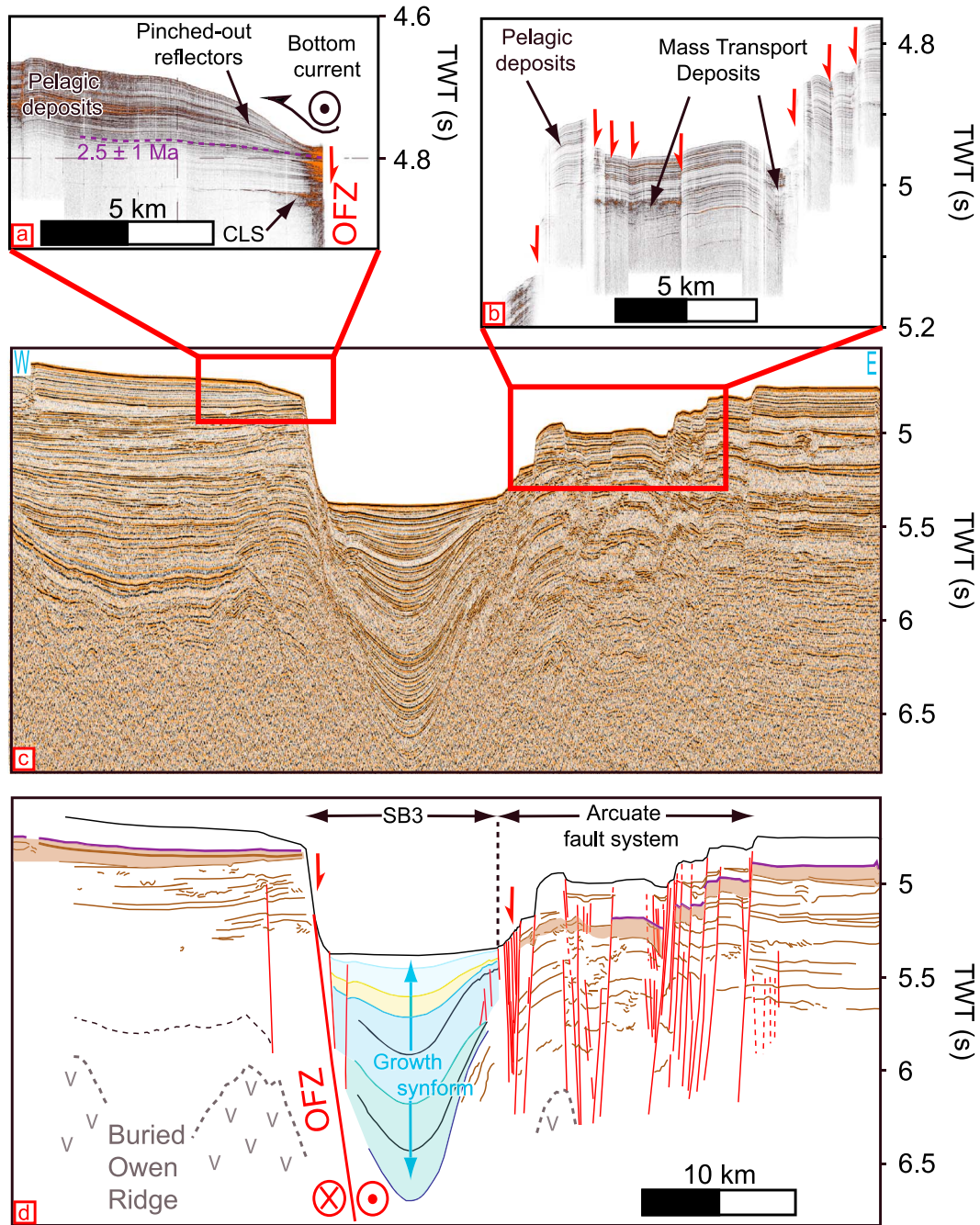
Figure 5. (a) A 3.5 kHz profile showing the influence of bottom current on sediment architecture on the western edge of the 20°N Basin. (b) 3.5 kHz profile crossing the arcuate normal fault system. (c) Seismic line transverse to SB3 and (d) the related interpretation. See Figure 1 for location and Figure 2 for stratigraphic captions. OFZ: Owen Fracture Zone, SB: subbasin.

3. Stratigraphic Framework

[14] Correlation of seismic horizons documents the timing of faulting and folding through dating based upon sedimentation rates or relative chronology dating. The correlation of 20°N Basin deposits also documents periods of connection between subbasins controlled by the competition between sedimentation and structure growth. The data set partially images the depth of the substratum of the 20°N Basin, i.e., the depth of the last Indus channel-levee system deposited before

its opening (Figure 2). The stratigraphic ages of major chronologic markers are summarized in Figure 2 (inset c) and Table 1.

3.1. Identification of Sedimentary Deposits

[15] The identification of sedimentary deposits in the 3.5 kHz and seismic profiles is based on their seismic characters and correlation with DSDP site 222 [*Shipboard Scientific Party*, 1974] and Küllenberg cores from *Bourget et al.* [2013] (see Figure 1 for location). Turbiditic deposits are observed in all seismic profiles crossing the Owen and Indus abyssal

Table 1. Conversion of the Thickness of Pelagic Deposits Into Time

	Age estimates (in Ma) considering a 46m/Ma sedimentation rate	Age estimates (in Ma) considering a 30 m/Ma sedimentation rate
Thickness of pelagic deposits overlying the last active CLS : 0.14–0.16 s (TWT)	2.33–3.01	3.57–4.61
Thickness of pelagic deposits corresponding to the onset of contouritic deposits : 0.09–0.12 s (TWT)	1.56–2.29	2.4–3.52
Thickness of pelagic deposits overlying the C3 reflector : 0.08 s (TWT)	1.38–1.56	2.12–2.39

plains, in agreement with DSDP site 222 [*Shipboard Scientific Party*, 1974]. Indus Fan sedimentation started during the Middle Eocene and accelerated since the Early Miocene until Pleistocene in the area of the 20°N Basin [*Clift et al.*, 2001; *Clift*, 2002].

[16] The arcuate fault system east of SB3 affects a complex sequence of channel-levee systems. They display well-stratified horizons with successions of high- and low-amplitude reflections on 3.5 kHz and seismic profiles (Figures 2–5). Turbiditic processes commonly form channel-levee systems that are easily detectable (inset in Figure 2a). Channel axes are characterized by a typical lens-like architecture with a concave-up lower boundary and discontinuous, high-amplitude reflections. The associated levees display a wedge shape, high amplitude, and transparent seismic facies. Migration of the channel axis is indicated by lateral shifts of the channel infill facies. In the area of the 20°N Basin, a Pleistocene pelagic drape overlies fossil turbiditic channels observed in the Indus and Owen abyssal plains. The pelagic drape has preserved their morphology over millions of years (Figures 2–5) [*Shipboard Scientific Party*, 1974; *Rodriguez et al.*, 2011]. Pelagic deposits display well-stratified, continuous, and conformable horizons on 3.5 kHz profiles (Figures 3–5), which sometimes mimic the turbiditic facies. The pelagic drape is composed of detrital clay nanno-ooze to nanno-rich detrital carbonate silty clay (DSDP site 222) [*Shipboard Scientific Party*, 1974]. A pelagic facies is also observed in the uppermost section of the SB1 and SB2. Additionally, some mass transport deposits are occasionally observed at the edge of some faults of the arcuate system (Figure 4). They display a typical chaotic to transparent facies on both 3.5 kHz and seismic data.

[17] Deep-sea currents disturbed by the topography of the 20°N Basin influenced the architecture of the pelagic cover at the edges of the 20°N Basin. Deep-sea currents typically induce significant lateral thickness variations related to lateral gradients of current velocity and geometric discontinuities related to variations of current activity through time. Typical sigmoid geometries composed of reflectors nonparallel to the accumulation surface [*Faugères et al.*, 1999; *Faugeres and Mulder*, 2011] are observed on the western edge of the 20°N Basin (Figure 5) and over some of the arcuate normal faults to the east (Figure 4).

[18] Subbasin 3 displays particularly thick and transparent sedimentary layers on seismic profiles, with strong lateral thickness variations (Figures 2, 4, and 5). This facies corresponds to turbiditic deposits according to Küllenberg core analysis [*Bourget et al*, 2013]. Ponded turbidites are commonly observed in pull-apart basins (e.g., pull-apart basins in the Marmara Sea) [*McHugh et al.*, 2006; *Beck et al.*, 2007] since they represent very restricted areas of deposition in comparison to abyssal plains. The volume of the turbiditic plume,

usually spread over large surfaces, is thus confined and the plume material is submitted to oscillations, leading to strong sediment sorting. Coarse grains are deposited at the bottom of the sequence and favor high-amplitude reflection, whereas the muddy part of the flow concentrates and produces the observed thick, transparent facies on seismic profiles. A typical characteristic of such deposits is that they can smooth and flatten the preexisting topography if voluminous enough (Figure 2).

3.2. Age of the 20°N Basin

[19] Several fossil turbiditic channels coming from the Indus fan [*Rodriguez et al.*, 2011] are observed at the seafloor on both sides of the 20°N Basin (i.e., west and east, Figure 1). Assuming they were traveling in the abyssal plain, traces of their activity should predate the opening of the 20°N Basin and therefore give its maximal age. Consistently, the last folded layer on the western side of SB2 (Figure 3) is formed by a channel-levee system. Seismic reflection profiles show that faulted fossil channel-levee systems located on both the western and eastern side of the 20°N Basin are covered by a 0.14–0.16 s (TWT) thick pelagic drape (corresponding to 105–140 m) (Figures 4 and 5). DSDP site 222 and ODP site 722 sedimentation rates [*Shipboard Scientific Party*, 1974, 1989] range between 30 and 46 m Ma^{-1} for the Pleistocene interval, which gives a ~3.4 ± 1.2 Ma age of deactivation of the channels (Table 1). Traces of late activity of the turbiditic channels found east of the 20°N basin (Figure 3) can be dated at 1.1 ± 0.2 Ma using the same method. The important clue is that these turbidites are not found on the opposite (western) side of the basin, the depression acting as a topographic barrier.

[20] The sigmoid pattern in the pelagic sediments at 4.8 s (TWT) on the western edge of the OFZ (Figure 5) probably indicates a local reorganization of the deep-sea currents at the onset of the drastic subsidence at SB3. Thus, the age of opening of the 20°N Basin, i.e., the age of a well-developed topographic step along the OFZ, can be estimated independently by dating the last pelagic layer unaffected by bottom current at 4.8 s (TWT). Through seismic correlation (Figure 5a), we measured the pelagic thickness overlying the 4.8 s (TWT) reflector in an area unaffected by bottom currents further west in the Owen Basin. The 0.09–0.12 s (TWT) thick cover measured on the western side of the basin (Figure 5a) indicates an age of 2.5 ± 1.0 Ma according to DSDP-ODP sedimentation rates (Table 1). Using the age of cessation of activity of the channels and the age of initiation of the contouritic deposits, we conclude that the opening of the 20°N Basin started around ~3 Ma.

3.3. Identification of the Substratum of the 20°N Basin

[21] The identification of a buried channel-levee system within the 20°N Basin gives the maximal depth of the substratum. The
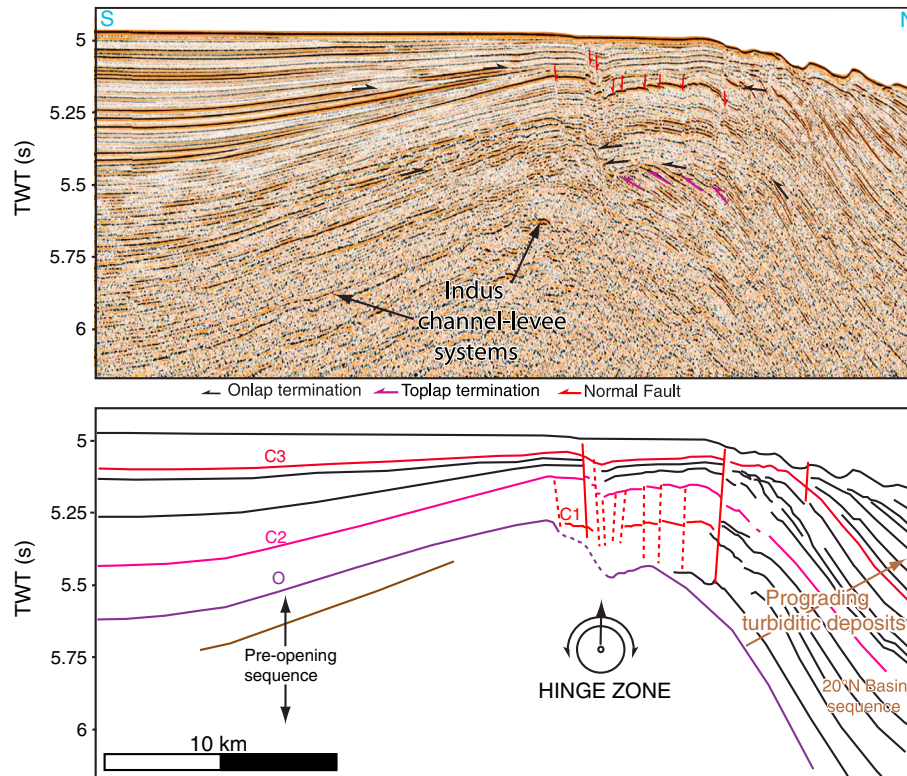
Figure 6. Close view of the longitudinal seismic profile crossing the hinge zone between SB2 and SB3. See Figure 2 for location and for stratigraphic captions.

assumed depth of the substratum (i.e., preopening strata) is labeled "O" (which stands for Opening) and picked in purple on seismic lines. The age of the substratum is assumed to be the same as the age of the opening of the basin, i.e., ~3 Ma. In the area of SB1, a channel-levee system from the Indus fan is identified at ~5.3 s (TWT), which must be considered as the maximal depth of the substratum of SB1. The last active channel-levee system identified west of SB2 (Figure 3) can be confidently correlated within the basin. Its top marks the maximal depth of the substratum. Below this key O reflector, the dip of the reflectors is rather constant; local and limited lateral thicknesses variations are due to fossil channel-levee systems of the Indus fan. This contrasts with the growth fold configuration observed above the O reflector (Figures 2 and 6), which indicates active and long-lived subsidence.

[22] The substratum of SB3 was not reached. An angular unconformity is observed between 5.3 and 5.7 s (TWT) in the area of the transverse fault system between SB2 and SB3 (Figures 2 and 6). This surface is evidenced by top lap terminations of the underlying deposits (Figure 6). The overlying deposits adopt an onlap configuration over the unconformity (Figures 2, 3, and 6). Although difficult to pick because of the density of faulting, this unconformity seems to correlate fairly well with the substratum of SB2. It indicates that the unconformity marks the onset of subsidence of SB2 and SB3 together with the beginning of growth folding along the hinge zone between SB2 and SB3.

3.4. The Sedimentary Infill of the 20°N Basin

[23] The present-day feeder channel of the 20°N Basin incises the arcuate fault system to the east (Figures 1 and 4).

Close-by channel-levee systems are all inactive since the opening of the basin, which implies that the present-day feeder has been the only turbiditic route to the basin. The depth of the thalweg has preserved the feeder channel from major avulsion during the last million years. The longitudinal seismic profile across the 20°N Basin (Figure 2) shows that recent turbiditic deposits are confined in the northern part of SB3 (which is the depocenter) and that the southern part of SB3, SB2, and SB1 are currently isolated from turbiditic deposits since the reflector picked in yellow (named AU2 in Figure 2). This reflector is about 120 ka old according to the correlation with a Küllenberg core collected within SB3 [*Bourget et al.*, 2013]. The overlying reflectors display a pinched-out configuration toward the south and end abruptly on the tilted topography created by a transverse growth fault (Figure 2). In subrecent times, the topography accumulated by this growth fault activity has exceeded the sedimentary supply, leading to the disconnection of the southernmost part of SB3 (Figure 2). Because of the progressive tilting of the sedimentary layers through times in each subbasin, one should consider that the deepest tilted horizons in the present-day configuration were nearly flat when deposited.

[24] At least seven angular unconformities are identified within SB3 (labeled AU1 to 6 and C3, Figures 2, 4, and 5) and indicate periods of turbiditic starving, promoting disconnection within SB3 compartments. Similarly, the growth of the hinge zone between SB2 and SB3 promoted the disconnection of these subbasins, currently blanketed by pelagic deposits [*Rodriguez et al.*, 2011]. The thickness of deposits above the substratum of SB1 and SB2 (reflector O) is much larger than what would be expected with pelagic processes
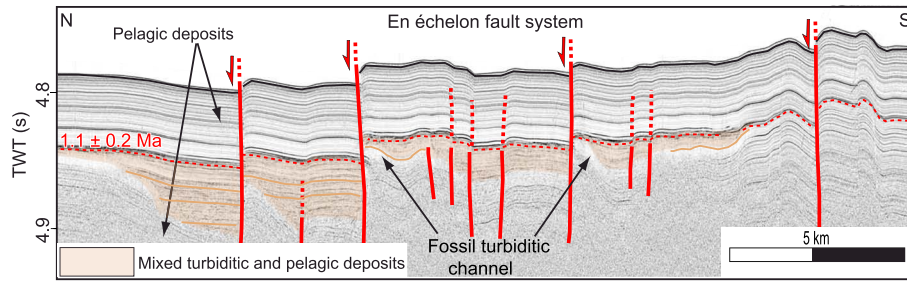
Figure 7. A 3.5 kHz profile crossing the en echelon fault system. See Figures 1 and 3 for location.

alone (0.1 s corresponds to 1.4–1.7 Ma according to DSDP site 222 sedimentation rates). This suggests periods of turbiditic deposition in SB1 and SB2, i.e., connection with SB3. Four sedimentary units can be distinguished within SB2 since the opening of the basin and interpreted in terms of episodes of connection or disconnection with SB3.

[25] 1. The first unit is delineated by the discontinuity O on the bottom and the red reflector (labeled C1) on the top (Figure 2).

[26] 2. The second unit (between reflectors C1 and C2) shows a constant thickness and can be correlated toward the SB3.

[27] 3. The third unit is delineated by the pink reflector (labeled C2) on the bottom and the dark red reflector on the top (labeled C3) (Figure 2).

[28] 4. The fourth unit is defined by the reflector C3 at the bottom and the topography.

[29] In the deepest part of the hinge zone, sediments belonging to SB3 onlap the unconformity O (referred to as the substratum of the 20°N Basin) and end abruptly on a fault belonging to the hinge zone (Figures 2 and 6). In the hinge zone, the fault delineated by the abrupt termination of sediments might have acted as a topographic barrier and favored subbasin disconnection in the first stages of opening. The second unit is likely to mark the first episode of connection between SB2 and SB3. The correlation shows that an episode of connection between SB1 and SB2–3 occurred before the reflector C3. Unfortunately, we cannot precisely date when the connection between SB1 and SB2 established. SB1 may have been in an elevated position with respect to SB2 until the time of reflector C2 and isolated from deposits coming from the feeder channel. The geometry of the third units is characterized by large lateral variations of layer thickness and pinched-out configuration of reflectors on the hinge zone (Figures 2 and 6) and the bounding faults (Figure 3). This configuration is very similar to what is observed on transverse growth structures in SB3 (Figure 2) and indicates a change in the sedimentation/topography growth balance. The seismic correlation of the longitudinal profile shows that the definitive disconnection between SB2 and SB3 occurred at the time corresponding to reflector C3 (at 5 s TWT) (Figure 2). According to the ~68 m thick overlying pelagic cover measured in SB1, this disconnection occurred ~1.8 ± 0.5 Ma ago.

4. Activity of Structures in the 20°N Basin

[30] Turbiditic processes provide frequent snapshots of fault activity by erasing the topography. In contrast, slow pelagic sedimentation rates do not exceed the rate of fault activity, which results in a permanent fault scarp [*Barnes and Pondard*, 2010]. In seismic, it may be difficult to recognize a fresh fault scarp (active fault) from a pelagic drape of an inactive scarp. The arcuate fault system on the eastern sidewall is dominantly covered by pelagic deposits, as shown by both 3.5 kHz and seismic profiles (Figures 4 and 5) [*Rodriguez et al.*, 2011]. However, mass transport deposits are observed at the edge of some fault scarps on multibeam, 3.5 kHz, and seismic data (Figure 5), whereas these are absent in the older sequences This strongly suggests that fault activity is responsible for mass failures. These mass transport deposits are about 1.2 ± 0.3 s (TWT) Ma old according to the thickness of the overlying pelagic cover, which indicates a minimal age of activity of the arcuate fault system. Further, the topographic profile running through the axis of the feeder channel displays several major knickpoints, which suggests that the arcuate fault system is still active [*Bourget et al.*, 2013]. The turbiditic infill of SB3 provides a good record of the activity of the numerous transverse growth faults. Only a few faults are inactive (dotted lines in Figure 2). The signification of angular unconformities within SB3 remains ambiguous. They could indicate either coeval periods of abrupt increase in fault activity or period of sediment starving. In the latter case, deformation is still accumulating on each fault during periods of nondeposition, but the record is discontinuous.

[31] The record of deformation in SB1 and SB2 is dependent upon episodes of connection with SB3. An undeformed pelagic cover seals the buried growth faults identified south of SB1 since the time of reflector C3 (~1.8 ± 0.5 Ma), i.e., the time of disconnection with SB3 (Figure 2). We cannot assess if the southernmost normal fault is active or if the fault scarp is simply preserved by the pelagic sedimentation. The latter observations cast doubts on the activity of subsidence in SB1 since the reflector C3. The growth fold geometry of SB2 is observed in the subsurface reflectors, which indicates that subsidence is still active in SB2, although at a very slow rate. The reflector C2 crossing the hinge zone marks an episode of deactivation of most of the faults between SB2 and SB3 (Figures 2 and 6). Only one major fault is still active in this area, indicating that subsidence is mostly accommodated by transverse growth faults within SB3 (Figures 2 and 6). The en echelon fault system located to the southeast of the 20°N Basin is also covered by a 1.1 ± 0.2 Ma old pelagic drape (Figures 7) [*Rodriguez et al.*, 2011]. However, the en echelon fault system offsets the last turbiditic deposits, indicating that faulting was active after 1.1 ± 0.2 Ma. Turbiditic deposits at ~1.1 Ma have partly smoothed the numerous half graben isolated by en echelon strands, but faults remained active after this episode.
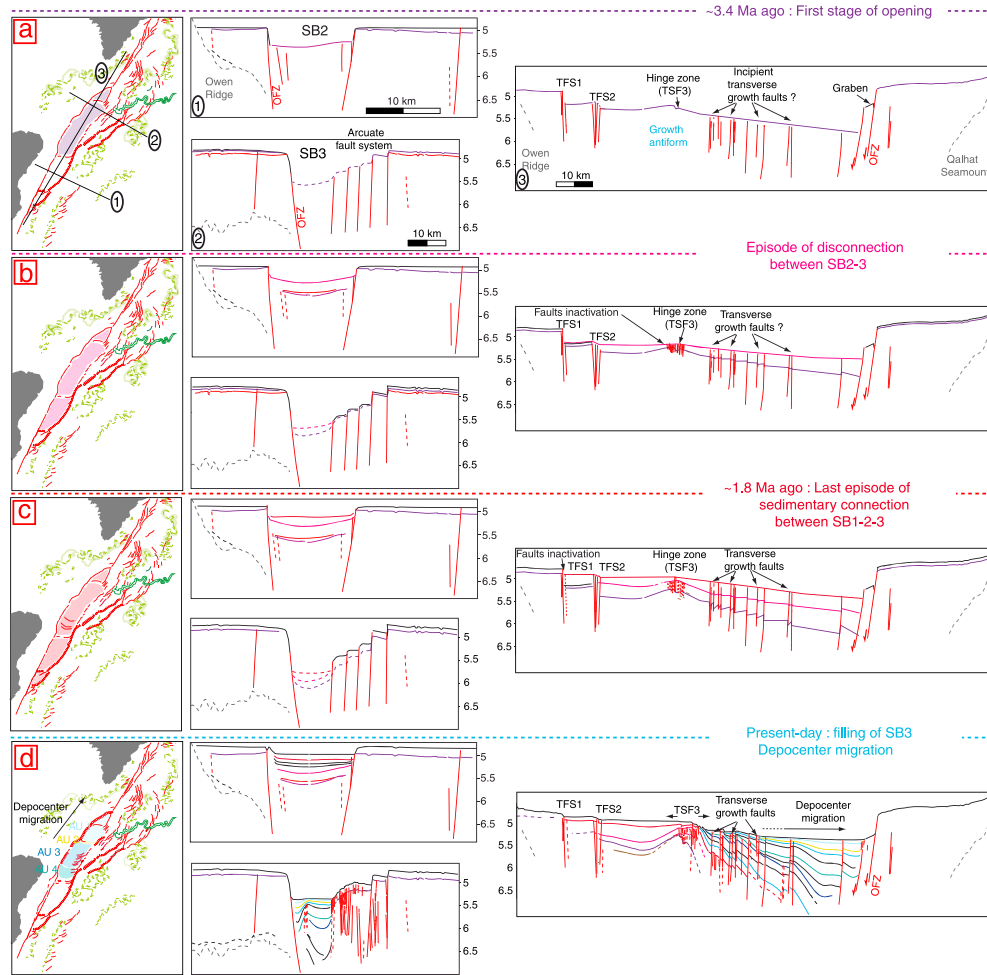
Figure 8. Synthesis of the structural evolution of the 20°N Basin. See discussion for details.

5. Discussion

5.1. History of the 20°N Pull-Apart Basin

[32] We propose a first-order chronology of the most probable structural evolution of the 20°N Basin and its sedimentary filling (Figure 8).

[33] 1. The study of channel-levee systems activity and bottom current deposits indicates that the 20°N Basin is at the most 3.4 ± 1.2 Ma old. The observation of contouritic deposits indicates that the topography related to the subsidence of the SB3 was already significant at 2.5 ± 1.0 Ma. Reflector C2 documents that all subbasins were already well formed at a time that cannot be strictly estimated but prior to 1.8 ± 0.5 Ma (age of reflector C3). Abrupt folding in SB2 sealed by the O discontinuity, together with progressive tilt of the overlying deposits, indicates that the hinge zone between SB2 and SB3 has been active since the very early stage of opening of the basin (Figure 6). It remains unclear whether SB1 stood as an elevated graben since the very early stage of opening or was formed subsequently. The length of the 20°N Basin was already close to the present-day one (i.e., ~80 km long) after less than one million years of development only. The precise age of activation of the en echelon fault system to the south remains unknown, but 3.5 kHz data show evidences for activity before 1 Ma. Analog models [*Tchalenko*, 1970; *Schlische et al.*, 2002] suggest that en echelon fault

systems take place in the first stages of structural evolution of strike-slip fault systems. Thus, the activation of the en echelon fault system might be synchronous or even earlier than the 20°N Basin inception.

[34] 2. During the first stage of basin infill, SB1 and SB2 were disconnected from SB3 by a topographic barrier formed by the transverse fault system between SB2 and SB3 (labeled TFS3 in Figure 2). The first deposits of SB3 steeply terminate on this topographic barrier (Figure 6). The unit deposited between C1 and C2 marks the first episode of sedimentary connection between SB2 and SB3. The reflector C2 (between ~3.3 and ~1.8 Ma) marks several geological changes. First, numerous faults of the hinge zone were deactivated at that time (Figures 2 and 6). Second, the overlying sedimentary unit displays a fanning configuration, which might indicate a period of subbasin disconnection or sediment starving at the time corresponding to reflector C2. Third, it appears that connection between SB1 and SB2 occurred shortly before C2.

[35] 3. Reflector C3, which is 1.8 ± 0.5 Ma old, corresponds to the definitive disconnection between SB1–SB2 and SB3 (Figure 6). It also coincides with fault deactivation in the southernmost part of SB1. Since 1.8 ± 0.5 Ma, SB1 and SB2 are blanketed by pelagic deposits only.

[36] 4. Growth faults within SB3 seem to have been active before 1.8 ± 0.5 Ma, although we cannot assess the precise time

of their activation, neither their connection to the substratum. Only a few of them were deactivated at the time corresponding to reflector AU5. Several episodes of isolation of the southernmost part of SB3 from turbiditic deposits occurred. The present-day depocenter is restricted to the northern part of SB3 since ~120 ka according to calibration with a Küllenberg core [*Bourget et al.*, 2013], but it used to cover a greater part of the SB3 before. In the present-day configuration, growth faults within SB3, the arcuate fault system, and the transverse fault systems between SB1–SB2 and SB2–SB3 show evidences of activity.

[37] Some remaining uncertainties remain with regard to the present-day state of activity of some of the faults (the fault bounding the southern extremity of the SB1 and the en echelon fault system), the precise depth of the substratum in SB3, and the precise age of some sedimentary discontinuities. However, the summary exposed above must be considered as the most likely structural evolution of the 20°N Basin.

5.2. The Indus Turbiditic System and the Sedimentary Filling of the 20°N Basin

[38] The 20°N Basin has been dominantly filled in by turbiditic deposits from the present-day active channel since the first stage of opening, other surrounding channels being deactivated shortly before the opening. This highlights the exceptional longevity of this turbiditic channel (at least ~1.8 Ma and most probably ~3 Ma), whose deep incision has precluded major avulsion processes through times. The filling of the 20°N Basin is ruled by the competition between tectonic activity and sedimentation rates. Episodes of subbasins disconnection document periods of time during which the topography accumulated by the transverse growth structures exceeds the rate of sedimentation. Conversely, episodes of connection evidence periods where the rate of sedimentation exceeds the accumulated topography. Several sequence stratigraphy works document glacio-eustatic sea level changes and subsequent positions of the deltaic shoreline as the main control factors of the Indus fan sedimentation during the Pleistocene, turbiditic sedimentation being enhanced during sea level lowstands and reduced during highstands [*Posamentier et al.*, 1989; *Kenyon et al.*, 1995; *von Rad and Tahir*, 1997; *Prins et al.*, 2000; *Prins and Postma*, 2000; *Posamentier and Kolla*, 2003; *Catuneanu et al.*, 2009; *Bourget et al.*, 2013].

[39] Angular unconformities observed within SB2 and SB3 might indicate either an abrupt and episodic increase in faulting/folding rate linked to irregularities in the subsidence rate or a hiatus in the sedimentary record of deformation. Sandbox experiments show that the evolution of rollover structures similar to SB3 does not produce abrupt and cyclic episodes of increased deformation, although the deformation may not be steady state [*Mauduit and Brun*, 1998]. The apparent cyclic and periodic pattern of angular unconformities observed in SB3 might rather correspond to glacio-eustatic episodes of sediment starving related to sea level highstands. The upward decrease of the apparent thickness of sedimentary layers within sequences delineated by angular unconformities is in good agreement with the progressive reduction of the quantity of sediment available on the Indian continental shelf as expected during sea level lowstand periods [*Catuneanu et al.*, 2009].

5.3. Mode of Opening of the 20°N Pull-Apart Basin

[40] Since the first stage of opening of the 20°N Basin ~3 Ma ago, the OFZ has accommodated only 10–12 km of relative motion between India and Arabia [*Fournier et al.*, 2011]. This amount of relative motion drastically contrasts with the dimensions of the 20°N Basin, which questions the relationship linking the size of a pull-apart basin to the relative motion along the main strike-slip fault [*Aydin and Nur*, 1982; *Mann et al.*, 1983]. The opening of the 20°N Basin is characterized by the synchronous formation of three distinct subbasins since the very first stage of opening, which indicates that the dimension of the 20°N Basin did not significantly change with increasing slip along the OFZ. It implies that the amount of opening (i.e., the distance between the basin-bounding faults) is not equal to the amount of displacement along the OFZ. The formation of a step over area might have isolated a subsiding graben (corresponding to SB3, i.e., the main locus of subsidence), which subsequently underwent 10–12 km of distributed extension.

[41] Asymmetric subsidence accommodated by the OFZ formed a rollover structure in SB3 (Figure 2). Elsewhere, transverse profiles (Figures 4 and 5) do not show significant structural asymmetry, consistently with pure strike-slip motion along the OFZ [*Fournier et al.*, 2011]. The hinge zone between SB2 and SB3 is the major structure decoupling the subsidence between the subbasins, similar to what is observed in the Salton Sea along the San Andreas Fault [*Brothers et al.*, 2009].

[42] Where connection with the substratum is observed (SB1 and SB2), transverse faults do not seem to be inherited structures but new structures formed during the early stages of the 20°N Basin opening. Only one major episode of transverse fault abandonment is evidenced in the hinge zone, but a few of them are still active. The activity of transverse growth faults may have last at least since ~1.8 ± 0.5 Myr, as observed in SB3, indicating long-lived structures at the scale of the basin history. Most of the 10–12 km divergence was thus distributed over transverse fault systems, with a shift of their activity in SB3 as the hinge zone grew up. The huge amount of subsidence in SB3 has enhanced gravity-driven deformation over SB1 and SB2, as well as along the arcuate fault system (Figure 9).

5.4. Comparison With Analog Modeling Experiments

[43] The structures developed during the first stages of the step over formation are not well preserved for the 20°N Basin. However, analog models [*Dooley and Schreurs*, 2012] illustrate how a subsiding block can be isolated by the development of faults oblique to the main strike-slip direction connecting the two strike-slip segments bounding the step over area. The size and the shape of the isolated graben are dependent upon the distance between the two bounding strike-slip segments and their degree of overlap. The definitive isolation of the graben may mark the initiation of the rapid subsidence characteristic of pull-apart basins.

[44] The architecture of SB3 shows strong similarities with sandbox models simulating the development of rollover structures in salt tectonics [*Brun and Mauduit*, 2008]. According to these experiments, the development of a rollover structure requires a three-block system, i.e., two blocks that separate from each other on top of an extending
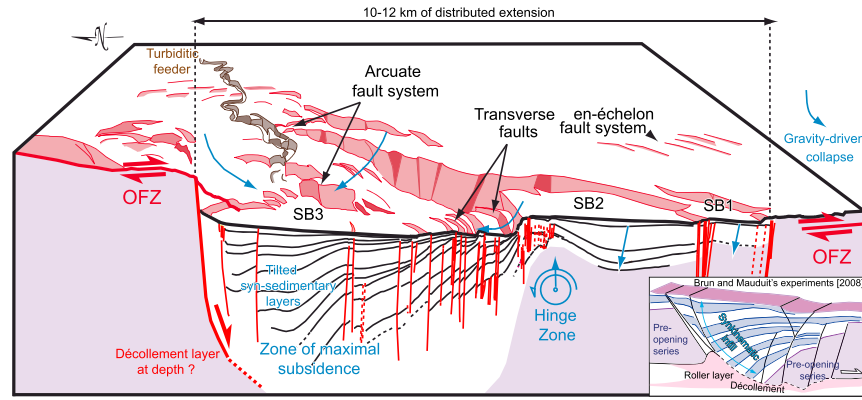
Figure 9. Schematic diagram showing subsidence in the 20°N Basin along the OFZ and the progressive tilting of sediments accommodated by a hinge zone. Arcuate normal faults, subbasins 1 and 2, transverse faults are the result of gravity-driven deformation in response to the high amount of subsidence accommodated by a rollover zone in subbasin 3. Inset on the right-hand corner shows results from sandbox experiments performed by *Brun and Mauduit* [2008].

décollement layer, isolating in between a third subsiding block [*Brun and Mauduit*, 2008]. Their experimental setup corresponding to a small amount of extension strikingly reproduces most of the structure of the 20°N Basin (see inset in Figure 9). The fanning configuration of deposits within SB3 and the upward curved geometry of the fault observed to the north of SB3 suggest that it connects to a décollement layer at depth. Numerous clay layers drilled in the Indus deep-sea fan [*Shipboard Scientific Party*, 1974, 1989] represent potential décollement layers at depth, whose thickness can control the subsidence of the basin. The growth of the 20°N Basin may thus result from gravity-driven deformation accommodated by a décollement layer at depth and enhanced by distributed extension in the area.

[45] On the other hand, results from experiments performed by *Smit et al.* [2008a] show that migration of subbasins and transverse fault initiation occur where the ratio between the step over wideness and the thickness of the deforming layer is <1. *Smit et al.* [2008a, 2008b] conclude that this ratio determines not only the basin width but also its geometry and the migration of subsidence. In these models, the intrabasin transverse faults appear during basin migration and do not result from the reactivation of inherited faults dividing the basin. In this framework, the migration of subsidence accounts for the growth of the pull-apart basin with increasing motion along the principal strike-slip fault. Although the experimental setup of models by *Smit et al.* [2008a, 2008b] applies well to the 20° N Basin, our proposed structural evolution does not show any evidence for subbasin or subsidence migration through times. Subbasins are delineated by newly formed transverse faults since the first stages of opening of the basin. The location of these transverse fault systems remained fixed, and they formed growing structural barriers that delineated areas of differential subsidence, the highest subsidence rates being recorded in SB3. Some of these faults may have become deactivated (for instance between SB2 and SB3), thus transferring larger amount of extension onto other preexisting transverse faults. *Ben Avraham and Ten Brink* [1989] showed that transverse faults within the Dead Sea formed as normal faults accommodating subsidence, subsequently submitted to strike-slip regime. A too important strike-slip component could lead to

the deactivation of the normal offset at transverse faults, but it could not be evidenced in the 20°N Basin.

5.5. Comparison With Other Pull-Apart Basins

[46] Intraoceanic pull-apart basins commonly occur along leaky transforms (e.g., the Siquieros transform fault in the Pacific [*Fornari et al.*, 1989] or the Andrew-Bain transform fault in the Indian Ocean [*Sclater et al.*, 2005]). Their size and their shape gradually evolve with increasing slip along the transform segments, ultimately giving birth to a spreading center that fill in the hole created by the pull-apart configuration (e.g., the Cayman Trough in Caribbean) [*Leroy et al.*, 1996; *Hayman et al.*, 2011]. This mode of opening is referred to as the "continuum model" [*Mann et al.*, 1983; *Mann*, 2007]. Direct comparison with the 20°N Basin is difficult because the step over is much more limited and the basin is nascent. The surprise is to see how closely the intraoceanic 20°N Basin compares with the continental Dead Sea Basin.

[47] Indeed, the dimension of the 20°N Basin is of the same order than that of the Dead Sea Basin (132 km long, 16 km wide). The Dead Sea Basin is also characterized by transverse faults delineating distinct subbasins of different depths [*Kashai and Croker*, 1987]. The major subsidence phase within the Dead Sea Basin started about 2–5 Ma ago, which would correspond to about 15–45 km of relative motion along the Dead Sea Fault [*Ginat et al.*, 1998; *Garfunkel and Ben-Avraham*, 2001; *Le Beon et al.*, 2008]. Finite motion along the OFZ since the opening of the 20°N Basin is less than the thickness of the deforming layer (oceanic crust plus sediments), which makes the 20°N Basin a nascent pull-apart basin, whereas the Dead Sea Basin is more mature [*Smit et al.*, 2008a]. This is related to the faster velocity along the Levant Fault, which is about twice that of the OFZ. Numerous conflicting modes of opening have been proposed [*Ten Brink and Ben-Avraham*, 1989; *Lazar et al.*, 2006], but the role of gravity-driven deformation in pull-apart growth has been previously invoked by *Ten Brink and Ben-Avraham* [1989] for the Dead Sea Basin. The latter also displays a longitudinal rollover structure formed by an upward concave fault (the Amazyahu Fault) rooting at depth on the salt layer of the Seldom formation acting as a

décollement layer [*Kashai and Croker*, 1987]. Seismic profiles [*Larsen et al*., 2002] and analog modeling experiments [*Smit et al*., 2008b] highlighted that the salt layer in the Dead Sea (Seldom fm.) mechanically decoupled the sedimentary infill from the basement structure. If the presence of a décollement layer in the 20°N Basin is confirmed, then the surface structure of the basin simply reflects gravity-driven deformation of the sedimentary cover in a narrow step over area (similarly to the Dead Sea) and does not reflect the pattern of the basement tectonics. Considering that the surface structures of the Dead Sea and the 20°N basins result from cover tectonics would explain why they compare so closely in spite of a different rheological setting.

5.6. Origin of the 20°N Basin

[48] The OFZ is associated with two large step over basins at its terminations, the Dalrymple Trough to the North (150 km long, 30 km wide) [*Edwards et al*., 2000] and the Beautemps-Beaupré Basin to the South (120 km long, 50 km wide) [*Fournier et al*., 2008a, 2008b]. As for the 20°N Basin, their large dimensions contrast with the estimated motion along the OFZ. However, the structural style of the OFZ terminations differs from the 20°N Basin. The OFZ forms a horsetail termination at the entrance of the Dalrymple Trough (characterized by a complex set of transverse faults) [*Fournier et al*., 2011; *Rodriguez et al*., 2011], whereas the Beautemps-Beaupré Basin displays a rhombohedric shape.

[49] The structural complexity of the OFZ between 20°N and 22°30′N contrasts with the "single-strand" pattern observed south of the 20°N Basin [*Fournier et al*., 2011; *Rodriguez et al*., 2011]. The 20°N Basin lies in the region of transition from the Arabian oceanic basin to the continental Laxmi-Palatina Ridge and the oceanic Gop Basin [*Minshull et al*., 2008; *Calvès et al*., 2011]. The increasing degree of complexity of the OFZ to the north may thus reflect the complexity of the nature and the properties of the adjoining lithospheres. The alternative is that the extensional component along the OFZ is gradually increasing to the north, as proposed in *DeMets et al*. [2010].

[50] Whether the opening of the 20°N Basin and the widening of the horsetail basins are coeval needs to be further investigated. Step over basins do not necessarily date the inception of strike-slip motion, since they were shown to develop a few million years after the initiation of the San Andreas Fault [e.g., *Wakabayashi*, 2007] and the Levant Fault [*Garfunkel and Ben-Avraham*, 2001]. An intriguing point is that the major episode of opening of the Dead Sea Basin along the Levant Fault [*Ten Brink and Flores*, 2012] is coeval with the structural reorganization of the OFZ. It remains unclear whether the opening of the Dead Sea reflects the mechanical evolution of the Levant fault or a kinematic change [*Schattner and Weinberger*, 2008; *Schattner*, 2010]. The coeval structural reorganization of both the Levant Fault and the OFZ may reflect a poorly constrained Pleistocene kinematic change of the Arabian plate motion [*Allen et al*., 2004].

6. Conclusions

[51] The 20°N Basin is a young asymmetric pull-apart basin initiated about 3 Ma ago along the slow India-Arabia transform plate boundary. The dimensions of this pull-apart (90 km long, 35 km wide) are strikingly large with regard to

the 10–12 km of finite motion accommodated since its inception. The subsurface structural evolution of the 20°N Basin may be assimilated to a rollover structure developing onto a décollement layer at depth in a narrow step over. Our understanding of the accommodation of the deformation in the deeper layers is still limited by the lack of gravity and deep seismic data. In spite of their different rheological setting, oceanic versus continental, the 20°N Basin may represent a good analog of the incipient stages of formation of the Dead Sea Basin. The presence of a décollement at depth, responsible for subsurface gravity-driven deformation decoupled from the crust, may explain the strong similarities between the superficial structure of the oceanic 20°N Basin and the continental Dead Sea Basin. The way the crust thins to accommodate the subsidence at the 20°N Basin remains enigmatic. *Ten Brink and Flores* [2012] recently emphasized that increased fluid flux in the continental crust beneath the Dead Sea might have enhanced the Pleistocene subsidence. An alternative is that the increase in subsidence resulted from a kinematic change along the Levant Fault [*Schattner and Weinberger*, 2008]. Kinematic changes drive step over reorganization along strike-slip boundaries. The local geometry of the step over is probably controlled by inherited rheological heterogeneities, determining *in fine* the dimensions of pull-apart basins. The rough synchronicity between the onset of both the 20°N and the Dead Sea basins suggests as a working hypothesis that the OFZ and the Levant faults recorded a Pliocene change in the Arabian plate motion.

References

Allen, M., J. Jackson, and R. Walker (2004), Late Cenozoic reorganization of the Arabia-Eurasia collision and the comparison of short-term and long-term deformation rates, *Tectonics*, 23, TC2008, doi:10.1029/2003TC001530.

Armitage, J. J., J. S. Collier, T. A. Minshull, and T. J. Henstock (2011), Thin oceanic crust and flood basalts: India-Seychelles breakup, *Geochem. Geophys. Geosyst.*, 12, Q0AB07, doi:10.1029/2010GC003316.

Aydin, A., and A. Nur (1982), Evolution of pull-apart basins and their scale independence, *Tectonics*, 1, 91–105, doi:10.1029/TC001i001p00091.

Barnes, P., and N. Pondard (2010), Derivation of direct on-fault submarine paleoearthquake records from high-resolution seismic reflection profiles: Wairau Fault, New Zealand, *Geochem. Geophys. Geosyst.*, 11, Q11013, doi:10.1029/2010GC003254.

Barton, P. J., T. R. E. Owen, and R. S. White (1990), The deep structure of the east Oman continental margin: Preliminary result and interpretation, *Tectonophysics*, 173, 319–331.

Basile, C., and J. P. Brun (1999), Transtensional faulting patterns ranging from pull-apart basins to transform continental margins: An experimental investigation, *J. Struct. Geol.*, 21, 23–37.

Beck, C., et al. (2007), Late Quaternary co-seismic sedimentation in the Sea of Marmara's deep basins, *Sediment. Geol.*, 199, 65–89.

Ben Avraham, Z., and U. S. Ten Brink (1989), Transverse faults and segmentation of basins within the Dead Sea Rift, *J. African Earth Sci.*, 8, 603–616.

Bourget, J., S. Zaragosi, M. Rodriguez, M. Fournier, T. Garland, and N. Chamot-Rooke (2013), Late quaternary megaturbidites from the Indus fan: Origin and stratigraphic significance, *Mar. Geol.*, *336*, 10–23, doi:10.1016/j.margeo.2012.11.011.

Brothers, D. S., N. W. Driscoll, G. M. Kent, A. J. Harding, J. M. Babcock, and R. L. Baskin (2009), Tectonic evolution of the Salton Sea inferred from seismic reflection data, *Nat. Geosci.*, *2*, 581–584, doi:10.1038/ngeo590.

Brun, J.-P., and O. Mauduit (2008), Rollovers in salt tectonics: The inadequacy of the listric fault model, *Tectonophysics*, *457*, 1–11.

Calvès, G., A. M. Schwab, M. Huuse, P. D. Clift, C. Gaina, D. Jolley, A. R. Tabrez, and A. Inam (2011), Seismic volcanostratigraphy of the western Indian rifted margin: The pre-Deccan igneous province, *J. Geophys. Res.*, *116*, B01101,doi:10.1029/2010JB000862.

Carton, H., et al. (2007), Seismic imaging of the three-dimensional architecture of the Cinarcık Basin along the North Anatolian Fault, *J. Geophys. Res.*, *112*, B06101, doi:10.1029/2006JB004548.

Catuneanu, O., et al. (2009), Towards the standardization of sequence stratigraphy, *Earth Sci. Rev.*, *92*, 1–33.

Chaubey, A. K., J. Dyment, G. C. Bhatthacharya, J.-Y. Royer, K. Srinivas, and V. Yateesh (2002), Paleogene magnetic isochrons and palaeo-propagators in the Arabian and Eastern Somali Basins, NW Indian Ocean, in *The Tectonic and Climatic Evolution of the Arabian Sea Region*, Geol. Soc. Spec. Publ., vol. 195, edited by P. D. Clift, pp. 71–85, Geological Society of London.

Christie-Blick, N., and K. T. Biddle (1985), Deformation and basin formation along strike-slip faults, in *Strike-Slip Deformation, Basin Formation, and Sedimentation*, Society of Economic Paleontologists and Mineralogists, Spec. Publ., vol. 37, edited by K. T. Biddle and N. Christie-Blick, pp. 1–35, Society of Economic Paleontologists and Mineralogists, California.

Clift, P. D. (2002), A brief history of the Indus River, in *The Tectonic and Climatic Evolution of the Arabian Sea Region*, Geol.Soc.Spec.Publ., vol. 195, edited by P. D. Clift, pp. 237–258, Geological Society of London.

Clift, P. D., N. Shimizu, G. D. Layne, J. S. Blusztain, C. Gaedicke, H. U. Schluter, M. K. Clark, and S. Amjad (2001), Development of the Indus Fan and its significance for the erosional history of the Western Himalaya and Karakoram, *Geol. Soc. Am. Bull.*, *113*(8), 1039–1051.

Cloos, E. (1968), Experimental analysis of Gulf Coast fracture patterns, *Am. Assoc. Pet. Geol. Bull.*, *52*, 420–444.

Collier, J. S., V. Sansom, O. Ishizuka, R. N. Taylor, T. A. Minshull, and R. B. Whitmarsh (2008), Age of Seychelles–India break-up, *Earth Planet. Sci. Lett.*, *272*, 264–277.

Cunningham, W. D., and P. Mann, (2007), Tectonics of strike-slip restraining and releasing bends, in *Tectonics of Strike-Slip Restraining and Releasing Bends*, Geol. Soc. Spec. Publ., *290*, edited by W. D. Cunningham and P. Mann, pp. 1–12, Geological Society of London.

DeMets, C., R. G. Gordon, D. F. Argus, and S. Stein (1990), Current plate motions, *Geophys. J. Int.*, *101*, 425–478.

DeMets, C., R. G. Gordon, D. F. Argus, and S. Stein (1994), Effect of recent revisions to the geomagnetic reversal time scale on estimates of current plate motions, *Geophys. Res. Lett.*, *21*, 2191–2194.

DeMets, C., R. G. Gordon, and D. F. Argus (2010), Geologically current plate motions, *Geophys. J. Int.*, *181*, 1–80, doi:10.1111/j.1365-246X.2009.04491.x.

Dooley, T., and G. Schreurs (2012), Analogue modelling of intraplate strike-slip tectonics: A review and new experimental results, *Tectonophysics*, *574-575*, 1–71.

Dyment, J. (1998), Evolution of the Carlsberg Ridge between 60 and 45 Ma: Ridge propagation, spreading asymmetry, and the Deccan-Reunion hotspot, *J. Geophys. Res.*, *103*, 24,067–24,084, doi:10.1029/98JB01759.

Edwards, R. A., T. A. Minshull, and R. S. White (2000), Extension across the Indian–Arabian plate boundary: The Murray Ridge, *Geophys. J. Int.*, *142*, 461–477.

Faugeres, J. C., and T. Mulder (2011), Contour currents and contourite drifts, in *Deep-Sea Sediments*, Developments in Sedimentology, vol. 63, edited by H. Huneke and T. Mulder, pp. 149–214, Elsevier, Amsterdam, The Netherlands.

Faugères, J. C., D. A. V. Stow, P. Imbert, and A. Viana (1999), Seismic features diagnostic of contourite drifts, *Mar. Geol.*, *162*, 1–38.

Fornari, D., D. Gallo, M. H. Edwards, J. A. Madsen, M. R. Perfit, and A. N. Shor (1989), Structure and topography of the Siquieros Transform Fault System: Evidence for the development of intra-transform spreading centers, *Mar. Geophys. Res.*, *11*, 263–299.

Fournier, M., C. Petit, N. Chamot-Rooke, O. Fabbri, P. Huchon, B. Maillot, and C. Lepvrier (2008a), Do ridge-ridge-fault triple junctions exist on Earth? Evidence from the Aden–Owen–Carlsberg junction in the NW Indian Ocean, *Basin Res.*, *20*, 575–590, doi:10.1111/j.1365-2117.2008.00356.x.

Fournier, M., N. Chamot-Rooke, C. Petit, O. Fabbri, P. Huchon, B. Maillot, and C. Lepvrier (2008b), In situ evidence for dextral active motion at the Arabia–India plate boundary, *Nat. Geosci.*, *1*, 54–58, doi:10.1038/ngeo.2007.24.

Fournier, M., et al. (2010), Arabia-Somalia plate kinematics, evolution of the Aden-Owen-Carlsberg triple junction, and opening of the Gulf of Aden, *J. Geophys. Res.*, *115*, B04102, doi:10.1029/2008JB006257.

Fournier, M., N. Chamot-Rooke, M. Rodriguez, P. Huchon, C. Petit, M.-O. Beslier, and S. Zaragosi (2011), Owen Fracture Zone: The Arabia–India plate boundary unveiled, *Earth Planet. Sci. Lett.*, *302*, 247–252, doi:10.1016/j.epsl.2010.12.027.

Garfunkel, Z., and Z. Ben-Avraham (2001), Basins along the Dead Sea transform, in *Peri-Tethys Memoir 6: Peri-Tethyan Rift/Wrench Basins and Passive Margins*, Mémoires Museum National d'Histoire Naturelle de Paris, *186*, edited by P. A. Ziegler, W. Cavazza, A. H. F. Robertson, and S. Crasquin-Soleau, pp. 607–627, Museum national d'histoire naturelle, service du patrimoine naturel, Paris, France.

Ginat, H., Y. Enzel, and Y. Avni (1998), Translocated Plio-Pleistocene drainage systems along the Arava fault of the Dead Sea transform, *Tectonophysics*, *284*, 151–160.

Hayman, N., N. Grindlay, M. Perfit, P. Mann, S. Leroy, and B. Mercier de Lépinay (2011), Oceanic core complex development at the ultraslow spreading Mid-Cayman Spreading Centre, *Geochem., Geophys., Geosyst.*, *12*, Q0AG02, doi:10.1029/2010GC003240.

Kashai, E. L., and P. F. Croker (1987), Structural geometry and evolution of the Dead Sea-Jordan rift system as deduced from new subsurface data, *Tectonophysics*, *141*, 33–60.

Kenyon, N. H., A. Amir, and A. Cramp (1995), Geometry of the younger sediment bodies of the Indus Fan, in *Atlas of Deep Water Environments: Architectural Style in Turbidite Systems*, edited by K. T. Pickering, R. N. Hiscott, N. H. Kenyon, F. Ricci Lucchi, and R. D. A. Smith, Chapman & Hall, London, pp. 89–90.

Larsen, B. D., Z. Ben-Avraham, and H. Shulman (2002), Fault and salt tectonics in the southern Dead Sea Basin, *Tectonophysics*, *346*, 71–90.

Lazar, M., Z. Ben-Avraham, and U. Schattner (2006), Formation of sequential basins along a strike-slip fault – Geophysical observations from the Dead Sea basin, *Tectonophysics*, *421*, 53–69.

Le Beon, M., Y. Klinger, A. Q. Amrat, A. Agnon, L. Dorbath, G. Baer, J.-C. Ruegg, O. Charade, and O. Mayyas (2008), Slip rate and locking depth from GPS profiles across the southern Dead Sea Transform, *J. Geophys. Res.*, *113*, B11403, doi:10.1029/2007JB005280.

Leroy, S., B. Mercier de Lépinay, A. Mauffret, and M. Pubellier (1996), Structure and tectonic evolution of the eastern Cayman Trough (Caribbean Sea) from seismic reflection data, *Am. Ass. Petrol. Geol. Bull*, *80*, 222–247.

Malod, J. A., L. Droz, B. Mustafa Kemal, and P. Patriat (1997), Early spreading and continental to oceanic basement transition beneath the Indus deep-sea fan: Northeastern Arabian Sea, *Mar. Geol.*, *141*, 221–235.

Mann, P. (2007), *Global Catalogue, Classification and Tectonic Origins of Restraining- and Releasing Bends on Active and Ancient Strike-Slip Fault Systems*, Geol. Soc. London Spec. Pub., vol. 290, pp. 13–142, Geological Society, London, Great Britain.

Mann, P., M. R. Hempton, D. C. Badley, and K. Burke (1983), Development of pull-apart basins, *J. Geol.*, *91*, 529–554.

Mauduit, T., and J.-P. Brun (1998), Development of growth fault/rollover systems, *J. Geophys. Res.*, *103*, 18,119–18,130.

McHugh, C. M. G., L. Seeber, M.-H. Cormier, J. Dutton, N. Cagatay, A. Polonia, W. B. F. Ryan, and N. Gorur (2006), Submarine earthquake geology along the North Anatolia Fault in the Marmara Sea, Turkey: A model for transform basin sedimentation, *Earth Planet. Sci. Lett.*, *248*, 661–684, doi:10.1016/j.epsl.2006.05.038.

Minshull, T., C. Lane, J. S. Collier, and R. Whitmarsh (2008), The relationship between rifting and magmatism in the northeastern Arabian Sea, *Nat. Geosci.*, *1*, 463–467, doi:10.1038/ngeo228.

Petrunin, A., and S. Sobolev (2006), What controls thickness of sediments and lithospheric deformation at a pull-apart basin?, *Geology*, *34*, 389–392, doi:10.1130/G22158.1.

Pondard, N., and P. M. Barnes (2010), Structure and paleoearthquake records of active submarine faults, Cook Strait, New Zealand: Implications for fault interactions, stress loading, and seismic hazard, *J. Geophys. Res.*, *115*, B12320, doi:10.1029/2010JB007781.

Posamentier, H. W., and V. Kolla (2003), Seismic geomorphology and stratigraphy of depositional elements in deep-water settings, *J. Sediment. Res.*, *73*, 367–388.

Posamentier, H. W., M. T. Jervey, and P. R. Vail (1989), Eustatic controls on clastic deposition I—Conceptual framework, in *Sea-Level Changes: An Integrated Approach*, SEPM Special Publication, edited by C. K. Wilgus, Society of Economic Paleontologists and Mineralogists, Tulsa, pp. 110–124.

Prins, M. A., and G. Postma (2000), Effects of climate, sea level, and tectonics unraveled for last deglaciation turbidite records of the Arabian Sea, *Geology*, *28*, 375–378.

Prins, M. A., G. Postma, J. Cleveringa, A. Cramp, and N. H. Kenyon (2000), Controls on terrigenous sediment supply to the Arabian Sea during the late Quaternary: The Indus Fan, *Mar. Geol.*, *169*, 327–349.

Rahe, B., D. Ferrill, and A. Morris (1998), Physical analog modeling of pull-apart basin evolution, *Tectonophysics*, *285*, 21–40, doi:10.1016/S0040-1951(97)00193-5.

Reilinger, R., et al. (2006), GPS constraints on continental deformation in the Africa–Arabia–Eurasia continental collision zone and implications for the dynamics of plate interactions, *J. Geophys. Res.*, *111*, B05411, doi:10.1029/2005JB004051.

Rodriguez, M., M. Fournier, N. Chamot-Rooke, P. Huchon, J. Bourget, M. Sorbier, S. Zaragosi, and A. Rabaute (2011), Neotectonics of the Owen Fracture Zone (NW Indian Ocean): Structural evolution of an oceanic strike-slip plate boundary, *Geochem. Geophys. Geosyst.*, *12*, Q12006, doi:10.1029/2011GC003731.

Rodriguez, M., M. Fournier, N. Chamot-Rooke, P. Huchon, S. Zaragosi, and A. Rabaute (2012), Mass wasting processes along the Owen Ridge (Northwest Indian Ocean), *Mar. Geol.*, *326-328*, 80–100, doi:10.1016/j.margeo.2012.08.008.

Rodriguez, M., N. Chamot-Rooke, H. Hébert, M. Fournier, and P. Huchon (2013), Owen Ridge deep-water submarine landslides: Implications for tsunami hazard along the Oman coast, *NHESS*, *13*, 417–424.

Royer, J. Y., A. K. Chaubey, J. Dyment, G. C. Bhattacharya, K. Srinivas, V. Yateesh, and T. Ramprasad (2002), Paleogene plate tectonic evolution of the Arabian and Eastern Somali basins, in *The Tectonic and Climatic Evolution of the Arabian Sea Region*, Geol. Soc. Spec. Publ., 195, edited by P. D. Clift, pp. 7–23, Geological Society, London.

Schattner, U. (2010), What triggered the early-to-mid Pleistocene tectonic transition across the entire eastern Mediterranean?, *Earth Planet. Sci. Lett.*, *289*, 539–548.

Schattner, U., and R. Weinberger (2008), A mid-Pleistocene deformation transition in the Hula basin, northern Israel: Implications for the tectonic evolution of the Dead Sea Fault, *Geochem. Geophys. Geosyst.*, *9*, Q07009, doi:10.1029/2007GC001937.

Schlische, R. W., M. O. Withjack, and G. Eisenstadt (2002), An experimental study of the secondary deformation produced by oblique slip normal faulting, *Am. Assoc. Petrol. Geol. Bull.*, *86*(5), 885–906.

Sclater, J. G., N. R. Grindlay, J. A. Madsen, and C. Rommevaux-Jestin (2005), Tectonic interpretation of the Andrew Bain transform fault: Southwest Indian Ocean, *Geochem. Geophys. Geosyst.*, *6*, Q09K10, doi:10.1029/2005GC000951.

Shipboard Scientific Party (1989), Site 731, *Proc. Ocean. Drill. Program Initial Rep.*, *117*, 585–652.

Shipboard Scientific Party, Site 222 (1974), In R.B. Whitmarsh, O.E. Weser, and D.A. Ross, DSDP Init. Repts, 23, doi:10.2973/dsdp.proc.23.106.

Smit J., J.-P. Brun, S. Cloetingh, and Z. Ben-Avraham (2008a), Pull-apart basin formation and development in narrow transform zones with application to the Dead Sea Basin, *Tectonics*, *27*, TC6018, doi:10.1029/2007TC002119.

Smit, J., J.-P. Brun, X. Fort, S. Cloething, and Z. Ben-Avraham (2008b), Salt tectonics in pull-apart basins with application to the Dead Sea Basin, *Tectonophysics*, *449*, 1–16.

Tchalenko, J. S. (1970), Similarities between shear zones of different magnitudes, *Geol. Soc. Am. Bull.*, *81*, 1625–1640.

Ten Brink, U. S., and Z. Ben-Avraham (1989), The anatomy of a pull-apart basin: Seismic reflection observations of the Dead Sea, *Tectonics*, *8*, 333–350.

Ten Brink, U. S., and C. H. Flores (2012), Geometry and subsidence history of the Dead Sea basin: A case for fluid-induced mid-crustal shear zone?, *J. Geophys. Res.*, *117*, B01406, doi:10.1029/2011JB008711.

Ten Brink, U. S., Z. Ben-Avraham, R. E. Bell, M. Hassouneh, D. F. Coleman, G. Andreasen, G. Tibor, and B. Coakley (1993), Structure of the Dead Sea pull-apart basin from gravity analyses, *J. Geophys. Res.*, *98*, 877–21,894.

von Rad, U., and M. Tahir (1997), Late Quaternary sedimentation on the outer Indus shelf and slope (Pakistan): Evidence from high-resolution seismic data and coring, *Mar. Geol.*, *138*, 193–236.

Wakabayashi, J. (2007), Stepovers that migrate with respect to affected deposits: Field characteristics and speculation on some details of their evolution, in *Tectonics of Strike-Slip Restraining and Releasing Bends*, Geol. Soc. Spec. Publ., 290, edited by W. D. Cunningham and P. Mann, pp. 169–188, Geological Society, London.

Wakabayashi, J., J. V. Hengesh, and T. L. Sawyer (2004), Four-dimensional transform fault processes: Progressive evolution of step-overs and bends, *Tectonophysics*, *392*, 279–301.

Wu, J. E., K. McClay, P. Whitehouse, and T. Dooley (2010), 4D analogue modelling of transtensional pull-apart basins, *Mar. Petr. Geol.*, *26*, 1608–1623.

Yatheesh, V., G. C. Bhattacharya, and J. Dyment (2009), Early oceanic opening off Western India-Pakistan margin: The Gop Basin revisited, *Earth Planet. Sci. Lett.*, *284*, 399–408.